1991-09

Reattachment Studies of an Oscillating Airfoil Dynamic Stall Flow Field

Ahmed, S.

AIAA 9th Applied Aerodynamics Conference, September 23-25, 1991 / Baltimore, MD
http://hdl.handle.net/10945/50449

AIAA 91-3225

Reattachment Studies of an Oscillating Airfoil Dynamic Stall Flow Field

S. Ahmed, MCAT Institute, San Jose, CA;
M. S. Chandrasekhara, Naval Postgraduate School and Navy-NASA Joint Institute of Aeronautics, Monterey, CA.

AIAA 9th Applied Aerodynamics Conference
September 23-25, 1991 / Baltimore, MD

Reattachment Studies of an Oscillating Airfoil Dynamic Stall Flow Field

S.Ahmed[1,3]
MCAT Institute, San Jose, CA 95127

and

M.S.Chandrasekhara[2,3]
Navy-NASA Joint Institute of Aeronautics,
Fluid Mechanics Laboratory, NASA Ames Research Center,
Department of Aeronautics and Astronautics,
Naval Postgraduate School, Monterey, CA 93943

Abstract

The reattaching flow over an oscillating airfoil executing large amplitude sinusoidal motion around a mean angle of attack of 10 degrees has been studied using the techniques of stroboscopic schlieren, two component laser Doppler velocimetry and point diffraction interferometry, for a free stream Mach number of 0.3 and a reduced frequency of 0.05. The results show that the dynamically stalled flow reattaches in a process that begins when the airfoil is very close to the static stall angle on its downward stroke and progresses over the airfoil through a large range of angles of attack as the airfoil angle decreases to about 6 degrees. The airfoil suction peak shows a dramatic rise as the static stall angle is approached and the velocity profiles develop such that the flow near the surface is accelerated. The process completes through the disappearance of a separation bubble that forms over the airfoil.

Nomenclature

C_p	pressure coefficient
$C_{p_{max}}$	maximum pressure coefficient
c	airfoil chord
f	frequency of oscillation, Hz
k	reduced frequency = $\frac{\pi f c}{U_\infty}$
M	free stream Mach number
U,V	velocity components in the x and y directions
U_∞	free stream velocity
$\|V\|$	absolute velocity
x,y	chordwise and vertical distance
α	angle of attack
α_o	mean angle of attack
α_m	amplitude of oscillation
γ	ratio of specific heats
ϵ	fringe number
ρ	density
ρ_r	density at reference conditions
ϕ	phase angle of oscillation
ω	circular frequency, radians/sec

1. Introduction

Flows over oscillating airfoils have received considerable attention with a view to improve the performance of the retreating blade of a helicopter. The retreating blade performance is limited by flow separation leading to dynamic stall. A comprehensive review of dynamic stall and its events is given by Carr[1]. The flow eventually reattaches later in the cycle and depending upon the mean angle of attack, amplitude and frequency of oscillations, a hysteresis loop of varying size develops, McCroskey[2]. It is known that the hysteresis loop determines the aerodynamic damping. Whereas extensive studies have been carried out on oscillating airfoils to understand the dynamic stall process, the reattachment of the unsteady separated flows has received little attention. Reattachment of unsteady separated flows is a topic of basic research in itself, as several issues of flow separation and attachment are involved, such as the local pressure gradient, the state of the separated shear layer and its ability to overcome the adverse pressure gradient and so on. An understanding of the process may also help in modifying the flow. For example., if the process can be completed rapidly, the airfoil can generate more lift through the cycle, thus altering its performance. The changes in the pressure distribution that occur over the airfoil may for some conditions cause limit cycle oscillation. A parameter based on the pitching moment of the airfoil (which in turn is dictated by the hysteresis loop) was defined[2] to determine the aerodynamic damping over the cycle of oscillation. It was observed that the damping could become negative during certain parts of the cycle resulting in an increase in the amplitude of oscillations leading to

[1] *Research Scientist; Member AIAA. On Leave from National Aeronautical Laboratory, Bangalore, India*

[2] *Assistant Director and Adjunct Research Professor; Associate Fellow, AIAA.*

[3] **Mailing Address: M.S. 260-1. NASA Ames Research Center, Moffett Field, CA 94035**

stall flutter. An understanding of the reattachment process is therfore essential to alleviate the stall flutter and improve the dynamic lift characterisitics of an oscillating airfoil.

Niven et al[3] made the first and only attempt to analyze the reattachment of separated flow of a two dimensional wing undergoing ramp-down motion through surface pressure measurements. This study showed that the reattachment process occurs over a finite length of time and the airfoil incidence at reattachment was found to be close to the static stall angle. However, no flow field measurements were available to understand the physics involved in the process. The present study at the Navy - NASA Joint Institute of Aeronautics being conducted in the NASA Ames Research Center, Fluids Mechanics Laboratory(FML) is aimed at understanding the mechanisms involved in the separation and reattachment of flows associated with oscillating airfoils through flow field analysis using a variety of experimental techniques. The experimental techniques used included the schlieren method for qualitative analysis of the global flow field, laser Doppler velocimetry (LDV) for quantitative measurements of the velocity field, and point diffraction interferometry (PDI) for measurements of density and pressure distributions.The initial studies of the dynamic stall problem were confined to the upstroke of the oscillation cycle to understand the mechanism of separation leading to the dynamic stall and the effects of compressibility on dynamic stall. Results of schlieren studies by Chandrasekhara and Carr[4] on an oscillating airfoil have indicated that compressibility effects set in at M=0.3. Further studies by Chandrasekhara and Ahmed[5] using LDV have shown the formation of a separation bubble near the leading edge prior to the formation of a dynamic stall vortex. Studies with the PDI technique by Carr et al[6,7] have confirmed the presence of a separation bubble and shown that the flow gradients are slow to develop in the oscillatory case compared to the steady state resulting in the delay of stall known as dynamic stall.

In this paper, results obtained on an oscillating NACA 0012 airfoil as it executes the downward stroke are presented. Flow field data obtained using three different experimental techniques are discussed and an attempt is made to describe the reattachment process of the separated flow field.

2. Description of the Experiment

2.1. Facility

The experiments were conducted in the FML Compressible Dynamic Stall Facility (CDSF). The CDSF is an indraft wind tunnel with a 35cm. X 25cm. test section. The oscillatory motion is produced by a drive system located on top of the test section connected to the test section windows by connecting rods on either side. The windows are mounted in bearings and the airfoil is supported between the windows with pins smaller than the local airfoil thickness. This provides optical access to the airfoil surface as well. Sinusoidal motion of the windows results in a sinusoidal variation of the airfoil angle of attack.

The drive is equipped with incremental position encoders that provide the airfoil instantaneous angle of attack and frequency/phase angle of oscillation. An absolute position encoder indicates the angle of attack. The specifications of the tunnel and drive system are:

$$\alpha = \alpha_o + \alpha_m \sin 2\pi ft = \alpha_o + \alpha_m \sin \omega t$$

$$0 \leq \alpha_o \leq 15^\circ$$

$$2^\circ \leq \alpha_m \leq 10^\circ$$

$$0 \leq f \leq 100Hz$$

$$0 \leq M \leq 0.5$$

$$200,000 \leq Re \leq 10^6$$

airfoil chord = 7.62cm.

The airfoil angle, reduced frequency and Mach number correspond to those of a helicopter in forward flight and the Reynolds number corresponds to that of a $\frac{1}{7}$th scale model rotor, whose test results are directly applicable to a helicopter rotor.

The tunnel is connected to a 240,000 CFM, 9,000 HP evacuation compressor that allows continuous running at all flow speeds. All other details of the system could be found in Carr and Chandrasekhara[8].

2.2. Measurement Techniques

Three different nonintrusive optical diagnostic techniques were used in the study. These were (A) stroboscopic schlieren (B) two component, frequency shifted and phase averaged LDV (C) stroboscopic point diffraction interferometry(PDI) and are described below.

A. Stroboscopic schlieren studies

Fig. 1 shows the schematic of the schlieren and LDV system used. A standard 3m. focal length mirror based schlieren system was set up in a 'Z' type configuration with a Xenon arc lamp light source at the focal length of one of the mirrors. The beam passing through the test section was focused on to a vertical knife edge and then imaging optics. The light source was triggered externally at the desired phase angles by an electronic circuit which compared the chosen phase angle of oscillation and the encoder data from the drive system and produced a TTL pulse when a match occured. No delays were found to be present between the events of matching the phase angle and the light flashing.

B. Unsteady flow LDV studies

A two color, two component, frequency shifted Argon-Ion laser based TSI system was used for velocity measurements. The system was operated 15° off-axis, in the forward scatter mode. Traversing was accomplished by directing the 4 beams on to a 352mm. focal length lens mounted on a computer controlled

traverse. The signals were processed by TSI 1990 counters.

Phase locking circuitry specially built for handling the random LDV data and the unsteady position data were used as an integral part of the data acquisition instrumentation. The LDV data was acquired in the coincidence mode as determined by a NASA LDV multiplexer, with the coincidence window-width arbitrarily chosen as $50\mu sec$. The coincidence pulse was used to trigger data acquisition and freeze the rapidly changing encoder values till data transfer to the computer could be completed. The schematic of the method used is depicted in Fig. 2. The software for data acquisition and processing included the standard tests of data validation, phase averaging by binning the data appropriately, identifying gaps in the data if the number of samples in any bin was less than a preselected value (50 in this case) and providing phase distributions of the velocity components. Any time the standard criteria were not satisfied, the data set was rejected and new data was acquired. Seeding was accompished by injecting $1\mu m$ polystyrene latex particles suspended in alchohol into the tunnel inlet. A minimum of 10,000 samples were collected per channel at each measurement point. The complete details of the scheme can be found in Chandrasekhara and Ahmed[5].

C. PDI studies

PDI is a real-time interferometry technique that uses fluid density changes to produce flow interferograms. Fig. 3 shows the schematic of the optical arrangement used. The optical arrangement is based on a standard schlieren system, with a pulsed Nd-YAG laser serving as the light source and a predeveloped photographic plate being used at the knife edge plane. The principle has been detailed in Ref. 6 and 7 and is only briefly described here. A pinhole is created (burned) *in-situ* in the photographic plate by increasing the laser energy, with no flow in the wind tunnel. This serves to act as a point diffraction source, producing spherical reference waves. When the flow is turned on, the cylinder of light passing through the test section experiences phase shifting depending upon the local flow conditions and the beam exiting the tunnel window focuses to a slightly larger spot around the pinhole. The portion of the light that passes through the pinhole loses all the phase information introduced by the flow due to the spatial filtering characteristics of the pinhole and thus becomes the reference wave. This reference wave subsequently interferes with the light that was transmitted around the pinhole through the photographic plate, creating real time fringe patterns, at the image plane of the optics system. Ref. 9 describes the other details of the actual implementation of the technique in the CDSF. In operation, the laser was triggered stroboscopically, as was done in the schlieren studies; a pulse generated by a photo diode that responds to the actual laser light pulse was used to freeze the encoder display to record the actual phase angle at which an interferogram was obtained.

2.3. Experimental Conditions

The flow Mach number was set to 0.3; the corresponding Reynolds number was 540,000. The oscillation frequency was 21.6 Hz, which corresponded to a reduced frequency of 0.05. The airfoil was oscillated about the 25% chord point, with its angle of attack varying as

$$\alpha = 10^\circ - 10^\circ \sin \omega t$$

The LDV probe volume was traversed in the range $-0.25 \leq \frac{x}{c} \leq 0.75$, $0.0 \leq \frac{y}{c} \leq 0.58$. The data to be presented and discussed will pertain to the downstroke and envelope angles of attack ranging from 20° to 0°.

3. Results and Discussion

The results are discussed in three parts. The first part contains flow visualization pictures obtained using the schlieren technique; the second part presents the LDV data in the reattaching phase of the flow; the results of the PDI studies are discussed in the last part.

3.1. Schlieren Studies

A. Steady flow behavior

Fig. 4 shows schlieren pictures of steady attached and separated flow fields on the NACA 0012 airfoil at M = 0.3. Fig. 4a was obtained for $\alpha = 12.33^\circ$ and it is clear that the flow is completely attached. In the picture, the dark region near the leading edge on the lower side represents the flow at the stagnation point. The white region following it shows density gradients due to the the acceleration of the flow through the suction peak. The dark patch after this is the region where a laminar separation bubble forms[7]. At high angles of attack, the boundary layer thickens considerably near the trailing edge, as can be seen in the figure. At one encoder count higher, $\alpha = 12.41^\circ$, the flow separates and this state is shown in Fig. 4b. The flow could be brought back to the attached state by simply returning to the lower angle of attack of 12.33°, demonstrating the very small hysteresis that was present in steady flow. The two pictures clearly demonstrate the abruptness of flow separation and reattachment in steady flow.

B. Unsteady flow behavior

Contrary to steady flow, reattachment in unsteady flows is a process occuring over a range of angles of attack (time). Fig. 5 presents stroboscopic schlieren pictures as the airfoil executes the downstroke sinusoidally from $\alpha = 20^\circ$ to $\alpha = 0^\circ$. At $\alpha = 20^\circ$, the flow is completely separated from the leading edge as seen in Fig. 5a. The only flow features to be noted are the stagnation point, the separated shear layer emanating from the airfoil leading edge and the trailing edge shear layer. For $\alpha = 13.82^\circ$, in Fig. 5b, the flow has begun to reattach around the

leading edge, but over most of the upper surface, it is still separated. A trailing vortex can be seen in the wake at about 10-15% chord distance from the trailing edge, which could be the starting vortex related to partial reattachment. This suggests that the airfoil has already begun to generate lift. At $\alpha = 10°$, Fig. 5c, the reattachment has progressed to about 10% chord from the leading edge. A trailing vortex is also present. But, the significant point of interest is the appearance of a dark region near the leading edge in the reattached flow. A dark region in the schlieren image represents deceleration for the knife edge orientation used in the present schlieren arrangement. Hence, on either side of this region, the flow is accelerating. It is believed that a separation bubble forms in this region, in which the leading edge boundary layer separates and then reattaches. Studies by Carr et al [7] have shown that a bubble forms on the upstroke of the airfoil and is still present at $\alpha = 10°$. It is interesting to note that, even in the downstroke, a similar feature is present, (see also Sec. 3.3). Fig. 5d presents the result for $\alpha = 6.1°$ and it is clear that the flow has reattached over the entire airfoil. However, a slight imprint of the separation bubble can still be observed at $\frac{x}{c} \simeq 0.15$ as the flow is accelerating on either side of this point. It was found that only for $\alpha < 6°$ the separation bubble was not present. This confirms that flow reattachment after dynamic stall is a process over a long range of angles of attack, $14° \geq \alpha \geq 6°$. Whereas the flow on the upstroke was attached for all these angles of attack, at corresponding angles of attack on the downstroke, the flow was still separated, indicating the presence of strong hysteresis effects in the flow.

3.2. LDV Studies

As stated in Sec. 2.3, the LDV measurements were carried out over $-0.25 \leq \frac{x}{c} \leq 0.75$ and $0.0 \leq \frac{y}{c} \leq 0.58$. The distributions of the absolute velocity obtained from these measurements are discussed below. Due to limitation of space, only selected data are presented.

A. Global distributions

The absolute velocity vector field at two angles of attack corresponding to the schlieren pictures in Fig. 5 are presented in Fig. 6. Fig. 6a shows velocity field at $\alpha = 20°$, when the airfoil is in the deep dynamic stall state. Also shown the edge of the shear layer for direct comparison with the flow visualization studies. At $\frac{x}{c} = -0.25$, the approaching fluid is accelerated at higher $\frac{y}{c}$ locations (for ex., $\frac{y}{c} = 0.4$ and higher), and the airfoil slows down the velocities along a streamline in line with it. The most notable feature is the large variation between the shear layer and the airfoil upper surface. The velocity reaches $0.5U_\infty$ at $\frac{x}{c} = 0.42$ and $\frac{y}{c} = 0.05$, whereas far higher ($0 \leq \frac{x}{c} \leq 0.75$, $\frac{y}{c} = 0.58$), the magnitude is about 1.1 - $1.2U_\infty$. It is also interesting to note that despite the large scale separation, no reverse velocities could be measured, even though frequency shifting was used in the LDV system. As the airfoil angle of attack decreases to 10°, the flow becomes partially attached up to $\frac{x}{c} \simeq 0.10$ and beyond this, the flow is still separated as can be seen from the schlieren picture in Fig. 5c. The absolute velocity profiles in Fig. 6b are nearly flat with a ensemble means of $1.1U_\infty$, in the region $0.17 \leq \frac{x}{c} \leq 0.42$, and perhaps this is due to the mixing in the region. This emphasizes that in unsteady flow, even gross separation does not necessarily imply reverse flow. Part of this could also be due to particles not following the rapid flow changes during the cycle in this high speed, high frequency and large amplitude dynamic flow. The velocity vector field at $\frac{x}{c} = 0.083$, further shows acceleration of the flow near the surface, where velocities of up to $1.35U_\infty$ are encountered. From the schlieren picture (Fig. 5c), this is the region where the flow reattaches through the bubble and therefore the acceleration seen is due to the reattachment. This process where the velocity near the surface exceeds the free stream as the flow redevelops continues while the flow reattaches over the airfoil.

B. Progression of the reattachment process

Fig. 7a and 7b show the velocity profiles at different angles of attack from the top of the stroke when the flow is completely separated to when full reattachment occurs at $\frac{x}{c} = 0.083$ and $\frac{x}{c} = 0.25$ respectively. Of interest are the velocity defect seen closer to the airfoil for $0.1 \leq \frac{y}{c} \leq 0.15$ in Fig. 7a and for $0.067 \leq \frac{y}{c} \leq 0.25$ in Fig. 7b. As the shear layer is still detached from the surface at $\alpha = 20°$ (Fig. 7a), the defect in the velocity profiles seen is due to the shear layer itself, with the lowest velocity being nearest to the airfoil. There is waviness in the profiles even at $\alpha = 12.59°$. This is believed to be due to the unsteady shear layer and also possibly due to an insufficient number of samples at certain locations and phase angles. Below this angle of attack, the profiles become smoother and the fluid layers closer to the airfoil surface are accelerated relative to those away from it, which indicates local reattachment. At $\frac{x}{c} = 0.25$ (Fig. 7b), the velocity defect is seen to be larger ($\simeq 0.3U_\infty$). The defect extends over a larger height above the airfoil and over other angles of attack as well, including $\alpha = 12.59°$. At $\alpha = 10.52°$, the velocity profile looks smooth. However, at $\alpha = 8.44°$, the distribution shows larger velocities near the surface indicating that the reattachment has progressed to this location. Further decrease in the angle of attack to $\alpha = 7.41°$ results in the establishment of a flow where the local velocities near the surface increase above the free stream value. The velocity profiles over the airfoil change from those with a defect to those in which the fluid is increasingly accelerated as the surface is approached through the reattachment process. Data at other $\frac{x}{c}$ locations confirmed this observation.

C. Comparison of velocity distributions on the up and downstrokes

Fig. 8a compares the velocity distributions at $\frac{x}{c} = 0.083$ at $\alpha = 10°$ on the upstroke and downstroke.

It is clear that the velocities on the upstroke are significantly higher, by as much as 20%. At $\frac{y}{c} = 0.083$, the decrease in the value observed on the upstroke is due to the formation of a bubble and has been discussed in detail by Chandrasekhara and Ahmed[5]. Whereas a bubble formed on the downstroke as well, measurements could not be obtained in it due to seeding difficulties (discussed in Ref. 5). Fig. 8b which compares the profiles at $\alpha = 5.46°$, on the upstroke and on downstroke, shows no difference between the cases compared, indicating the absence of hysteresis at this location. A comparison of the upper surface flow field at $\alpha = 10°$ on the upstroke and downstroke is made in Fig. 9a and 9b. The peak velocity reached is about $1.45U_\infty$ during the upstroke, while during the downstroke it is $1.35U_\infty$. Also, the velocity data for the downstroke shows low velocities of the order of $0.7U_\infty$ beyond 30% chord and the extent of, for example, $|V|=1.1U_\infty$ (the solid line in the figure) is nearly half that during the upstroke. Some of the differences between the upstroke and downstroke occur because of the hysteresis effects (due to the large scale flow separation). At $\alpha = 10°$, the flow is partially attached in the downstroke and fully attached in the upstroke. Thus, the changes seen could also be attributed to the the pressure effects induced by the moving airfoil. This implies that the pressure distribution over the airfoil is also significantly modified at the same angle of attack, a factor that needs to be included in any calculations of the flow if the forces and moments through the cycle are to be satisfactorily computed.

3.3. PDI Studies

A. Interpretation of Interferograms

The fringes seen in the interferograms are contours of constant density. The quantitative nature of interferograms enables computation of the pressure distribution over the airfoil when the flow is attached, using isentropic flow relations. In the present study, this assumption is carried through the boundary layer fringes also. It is believed that the changes due to the vortical nature of the flow in the thin boundary layer that forms do not significantly affect the nature of the distributions. The density along any fringe can be calculated from the Gladstone - Dale equation[10] for the present wind tunnel and laser used as

$$\rho - \rho_r = .009421\epsilon$$

where ϵ the fringe number is $0, \pm1, \pm2, \ldots$ for the bright fringes and $\pm\frac{1}{2}, \pm\frac{3}{2}, \pm\frac{5}{2}, \ldots$ for the dark fringes. Fringes from the free stream to the stagnation point have positive values. Hence, by simply counting the fringes from the stagnation point, the flow quantities along any fringe can be determined. The corresponding C_p distributions can be computed from the relation

$$C_p = \frac{\left[\left(\frac{\rho}{\rho_r}\right)^\gamma - 1\right]}{\left[\frac{\gamma}{2}M^2\right]}$$

Knowing the local density values, the corresponding local Mach number can be determined. In all the interferograms shown, the triangular pointers seen are the registration markers used for scaling and obtaining the pressure distributions. The apex of the left side marker is aligned with the airfoil leading edge and the line joining vertical edges of the two markers above and below the airfoil passes through $\frac{x}{c} = 0.25$.

B. Interferograms of the reattachment process

Representative interferograms of the reattaching flow during the downward motion of the airfoil are shown in Fig. 10. Flow stagnation is indicated by the point on the airfoil lower surface near the leading edge where all fringes can be seen to converge. In some figures, the stagnation point appears to be a region because each fringe has a finite width. The fringes in the shear layer show that the flow is separated from the leading edge. The white and black patches seen between the separated shear layer and the airfoil surface in Fig. 10a at $\alpha = 12.27°$ indicate pockets of constant density fluid. Separation at this angle of attack occurs from very near the leading edge. It is clear that the velocity variation in the shear layer is that corresponding to two dark fringes, which is about $0.15U_\infty$ (as determined by fringe counting) for the present experiment. In Fig. 10b, at $\alpha = 10.69°$, the flow has partially reattached. One of the dark fringes in the shear layer after following the acceleration around the leading edge has turned down toward the airfoil and merged the local boundary layer. However, by $\frac{x}{c} = 0.2$, the fringe once again lifts off from the surface, indicating separated flow from there on. By this stage, a few more fringes appear around the leading edge indicating further establishment of the flow there.

As the angle of attack decreases to 9.84°, in Fig. 10c, the flow reattachment has progressed to about 35% chord, beyond which it is still separated. At the same time the fringe pattern on the upper surface around the leading edge shows that all outer fringes are smoothly shaped, but those closer to the airfoil (between $\frac{x}{c} = 0.02 - 0.1$) after coming out radially become nearly parallel to the upper surface and drop vertically before merging with the boundary layer. This is due to the formation of a laminar separation bubble, an event that was found to occur during the upward stroke as well, Carr et al[7]. This can also be seen from Fig. 10b, but it is less definitive. However, the pressure distributions (see next section) in fact indicate that a bubble is present at $\alpha = 10.69°$ also. Eventually, by $\alpha = 8.01°$, in Fig. 10d, the bubble almost disappears.

It is interesting to note that on the upstroke, the bubble forms at an angle of attack greater than 5° and remains on the surface till the dynamic stall vortex forms at around the static stall angle[7]. The overall flow is still attached till dynamic stall occurs at $\alpha = 15.9°$. However, on the downstroke, the flow is partially separated and the bubble is present only at certain lower angles of attack, $\alpha < 12°$. This once again demonstrates the hysteresis effects of the large amplitude oscillation of the airfoil.

C. Pressure distributions during reattachment

The variation of the maximum suction pressure coefficient as a function of angle of attack on the NACA 0012 airfoil during the downstroke is plotted in Fig. 11. It shows that as reattachment progresses, the airfoil redevelops suction steadily, during a *decrease* in angle of attack, till $\alpha = 8°$. Once the flow has fully established around the airfoil, the suction peak drops, as the angle of attack decreases further, as can be expected. Of particular interest and importance is the initial steep increase in the peak suction level at $\alpha \approx 12.6°$. It should be noted that this airfoil stalls at $\alpha = 12.41°$, at M = 0.3 in steady flow, (see sec. 3.1). The flow gradients seem to adjust such that as the static stall angle is approached during the downstroke, the leading edge shear layer begins to reattach and then flow reattachment begins. A similar observation has been made by Niven et al[3] also in their study of the reattachment process during ramp-down tests on dynamic stall at various pitch rates. The details of the pressure distribution can now be studied to see the salient features of the reattachment process.

Fig. 12 presents the pressure distributions at various angles of attack during the downstroke. For $\alpha = 12.27°$, only a few fringes could be counted in the accelerating region (up to $\frac{x}{c} = 0.017$ till flow separation); the graph shows that the local $\frac{dC_p}{dx} \approx 500$. For $\alpha = 11.15°$, fringes were present in the adverse pressure gradient region beyond $\frac{x}{c} = 0.02$ as well. In between, however, the fringes could not be detected clearly. It can be seen that the suction peak, C_p decreases to -1.0 and then a pressure plateau forms till $\frac{x}{c} = 0.083$, after which the pressure drops steeply. Such a behavior is indicative of the presence of a separation bubble, in which a constant pressure region followed by pressure recovery exists. The length of the bubble cannot be determined exactly as its edges could extend beyond this point of increasing pressure as has been pointed by Tani[11]. Though the pressure distribution gives approximately the length of the bubble, determination of its precise size requires quantification of the stall behavior by other surface flow measurement techniques. It appears that for $\alpha = 10.69°$ and $\alpha = 10.31°$, there is little change in the distributions through the bubble, although the suction peak seems to increase. As the angle of attack decreases, the bubble grows as the boundary layer reattaches further downstream of the leading edge as can be seen from the wider extent of the plateau, for example, at $\alpha = 9.84°$. At the same time, the $C_{p_{max}}$ also decreases as flow development continues around the leading edge. At $\alpha = 8.01°$, kinks are still present in the C_p distribution up to $\frac{x}{c} = 0.13$. Thus, it is possible that a separation bubble is still present till after this location. However, at $\alpha = 4.16°$, the distribution is smooth and the bubble has disappeared. The peak C_p estimated from these interferograms was -1.7, but the actual $C_{p_{max}}$ is expected to be slightly higher (due to the difficulty of resolving the fringes in this region), whereas the $C_{p_{max}}$ for attached flow on the upstroke is -1.43 and -2.12 for steady flow, at $\alpha = 4.25°$. This supports the conclusion that reattachment is a quantitatively different process from the separating flow on the upstroke, even though qualititative similarity exists in regard to the formation of the bubble. The differences in the angles of attack between the upstroke and downstrokes for the suction peak and the bubble development are due to the hysteresis effects that are always present in these unsteady flows.

D. Comparison of LDV and PDI studies

Since two different quantitative measurement techniques were used in the present study, it is instructive to make a direct comparison of the methods and the results obtained. PDI provides a spanwise averaged instantaneous quantitative flow field picture whereas LDV yields a long time averaged point measurement of the flow. The Mach numbers derived from both methods are compared in Fig. 13 at $\alpha = 10°$, when the airfoil is undergoing downward motion. The solid lines shown in it are the contours corresponding to midpoint of the dark fringes of the interferograms and the dashed lines are the Mach contours obtained from LDV (for the corresponding fringe numbers). The agreement is good, considering the vastly different nature of the techniques. The cylinder of light used in PDI provides more data points closer to the airfoil surface, which was not possible with LDV because of the blockage of the beams by the oscillating airfoil. However, the agreement for those data that are coincident demonstrates the statistically stationary nature of the flow field in the region compared. It should be noted that major differences could appear in separated flow regions or in three dimensional flows.

Since LDV is a point measurement whose resolution is controllable, very detailed surveys of the flow could be obtained. The resolution of PDI is limited to the number of fringes that naturally form based on the laser wavelength, wind tunnel span and flow density changes. But, PDI offers flow field information instantaneously, obtaining this information would be a very time consuming task with LDV, a major consideration in high speed, forced, unsteady flows. The agreement obtained in this study enhances the confidence level of the results presented.

3.4. A Global Picture of the Reattachment Process

Based on the study, a picture of reattachment emerges, which is represented in Fig. 14. During deep dynamic stall of rounded leading edge airfoils, the separated shear layer always appears to emanate from around the leading edge. However, the separation point cannot be precisely determined. As the airfoil angle of attack decreases, the shear layer starts moving towards the airfoil upper surface, without any significant reattachment until the static stall angle is approached. Reattachment begins near the static stall angle; the subsequent flow development around the leading edge causes the suction pressure to increase sharply. The adverse pressure gradient following the peak suction causes the boundary layer to separate slightly downstream of the suction peak and the separated shear layer has its origin now at this point of separation. There is a moderate angle of attack range in which the flow remains partly

separated. The shear layer attaches to the surface forming a bubble, only when the angle of attack falls below the static stall angle ($\simeq 11^0$), but it once again separates further downstream, depending on the local flow conditions. As the reattachment region proceeds towards the trailing edge, the suction pressures continues to increase with the bubble still present. Eventually, when the flow completely attaches itself over the airfoil, and the angle of attack falls to about 5 degrees, the bubble disappears and the pressures near the leading edge starts to decrease. Contrary to steady flow, where the suction pressure decreases as the angle of airfoil is lowered, in dynamic condition, there appears to be an interaction between the two mechanisms of flow reattachment and flow due to positive angle of attack. During the reattachment process, the suction pressure continues to increase till the reattachment is completed. Beyond this the pressure decrease is due to the decrease in angle of attack only. If a mechanism is created for the reattachment to occur earlier, it is possible to reduce the hysteresis loop, and thus increasing the usable lift in the cycle. Though, this study has shed some light on the physics of the reattachment process, more studies are required to identify the effect of other parameters such as airfoil geometry on the reattachment process.

4. Conclusions

A detailed study of the reattachment process of dynamic stall flow over an oscillating airfoil has been carried out using three different optical techniques. The major conclusions from the study are:

1. Reattachment of the dynamic stall flow is a process unlike that in a steady flow.
2. LDV studies show that the velocity profiles change shape; profiles with a defect change to those in which the fluid layers are accelerated steadily as the airfoil surface is approached, as the reattachment progresses.
3. The process includes development of larger than free stream velocities near the airfoil surface as the process advances over it.
4. Reattachment begins at or near the static stall angle even in unsteady flow. As flow begins to reattach, the suction pressure coefficient rises rapidly, but its values are different from that in steady flow and the unsteady flow during the upstroke.
5. For the Reynolds number of the experiment, reattachment progresses through a separation bubble, which changes size during the process and disappears at a low angle of attack.
6. Good agreement was found between LDV and PDI studies, enhancing the confidence level of the measurements.

Acknowledgements

The work was supported by the Army Research Office grant (MIPR-ARO-132-90) to the Naval Postgraduate School and monitored by Dr. T.L. Doligalski. Additional support was provided by AFOSR (MIPR-91-0007) monitored by Maj. D. Fant and also by NAVAIR (monitored by Mr. T.S. Momiyama). The support provided by Dr. S.S. Davis, Chief, Fluid Dynamics Research Branch, the discussions with Dr. L.W. Carr, U.S. Army AVSCOM at FML and the software development contributions of Mr. P.J. Trosin, and the image processing help rendered by Mr. C. Boswell of Sterling Federal Systems are all gratefully acknowledged.

5. References

[1] Carr, L.W., "Progress in Analysis and Prediction of Dynamic Stall", *Jl. of Aircraft*, Vol. 25, No.1, Jan. 1988, pp. 6-17.

[2] McCroskey, W.J., "The Phenomenon of Dynamic Stall", NASA TM 81264, March 1981.

[3] Niven,A.J., R.A.McD. Galbraith and David,G.F Herring., "Analysis of Reattachment during Ramp Down Tests", *Vertica*, Vol 13, No.2, pp. 187-196, 1989.

[4] Chandrasekhara, M.S. and Carr, L.W. "Flow Visualization Studies of the Mach Number Effects on the Dynamic Stall of Oscillating Airfoils", *Jl. of Aircraft*, Vol. 27, No. 6, June 1990, pp. 516-522.

[5] Chandrasekhara, M.S., and Ahmed, S., "Laser Velocimetry Measurements of Oscillating Airfoil Dynamic Stall Flow Field", *AIAA Paper No. 91-1799*, Presented at the 22nd Fluid Dynamics, Plasma Dynamics and Lasers Conference, Honolulu, HI, June 24-26, 1991.

[6] Carr, L.W., Chandrasekhara, M.S., Ahmed, S. , and Brock, N.J., "A Study of Dynamic Stall Using Real Time Interferometry", *AIAA Paper No. 91-0007*, Presented at 29th Aerospace Sciences Meeting, Reno, NV, Jan. 7-10, 1991.

[7] Carr, L.W., Chandrasekhara, M.S. and Brock, N.J., "A Quantitative Visual Study of Unsteady Compressible Flow on an Oscillating Airfoil", *AIAA Paper No. 91-1683*, Presented at the 22nd Fluid Dynamics, Plasma Dynamics and Lasers Conference, Honolulu, HI, June 24-26, 1991.

[8] Carr, L.W. and Chandrasekhara, M.S., "Design and Development of a Compressible Dynamic Stall Facility", *AIAA Paper No. 89-0647*, to appear in *Jl. of Aircraft*.

[9] Brock, N.J., Chandrasekhara, M.S., and Carr, L.W., "A Real Time Interferometry System for Unsteady Flow Measurements", To be presented at *The 14th ICIASF Conference*, Rockville, MD, Oct. 25-27, 1991.

[10] Goldstein, R.J., "Fluid mechanics Measurements", *Hemisphere Publishing Corp.*, 1983.

[11] Tani, I., "Low Speed Flows Involving Bubble Separations", *Progress in Aeronautical Sciences*, Vol. 5, 1964, pp. 70-103.

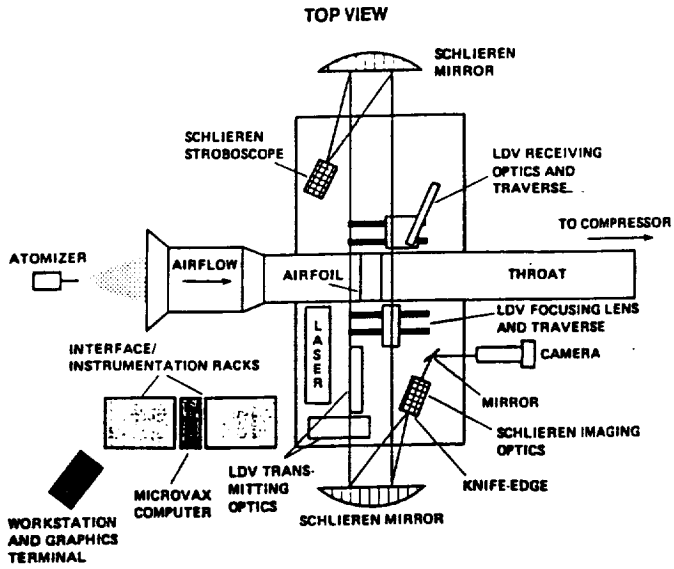

Fig. 1. Schematic of the CDSF Instrumentation.

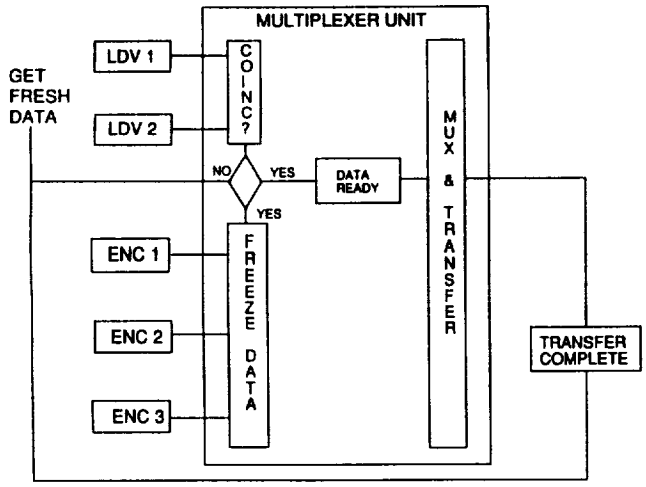

Fig. 2. Schematic of the LDV Data Acqusition Method.

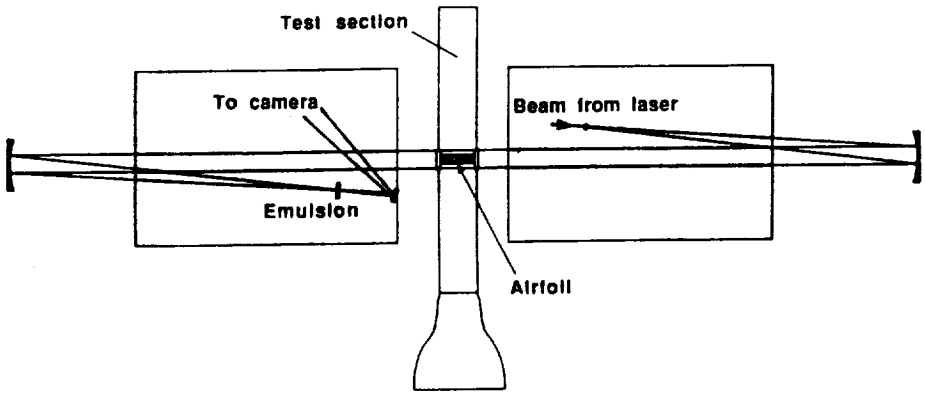

Fig. 3. Schematic of the Layout of Optics for Point Diffraction Interferometry.

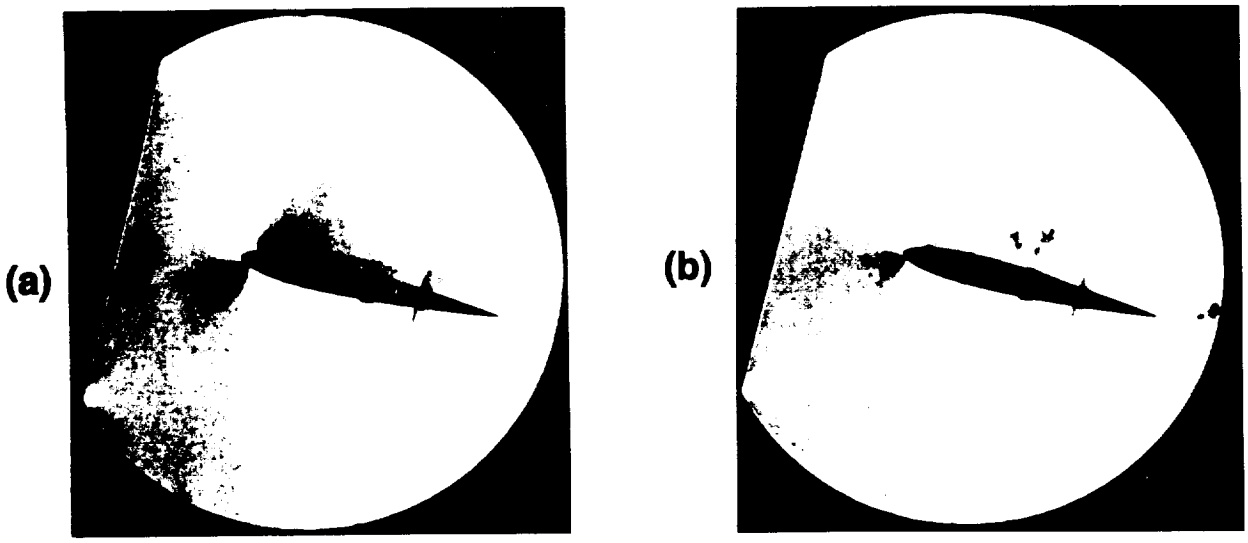

Fig. 4. Schlieren Photographs of the Steady Flow Behavior near stall: (a) $\alpha = 12.33°$, (b) $\alpha = 12.41°$.

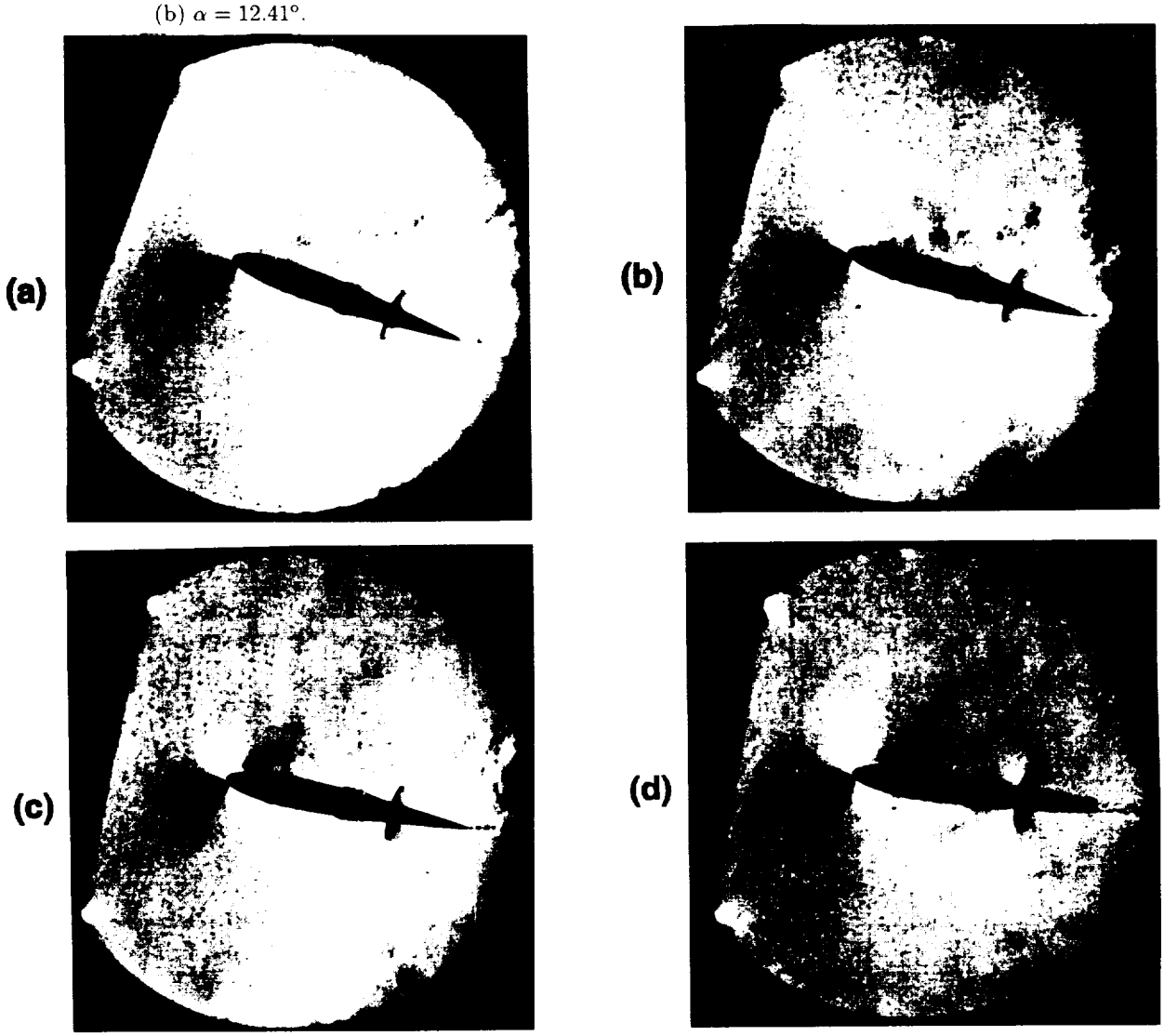

Fig. 5. Schlieren Photographs of Reattachment Process: (a) $\alpha = 20.0°$, (b) $\alpha = 13.82°$, (c) $\alpha = 10.0°$, (d) $\alpha = 6.17°$.

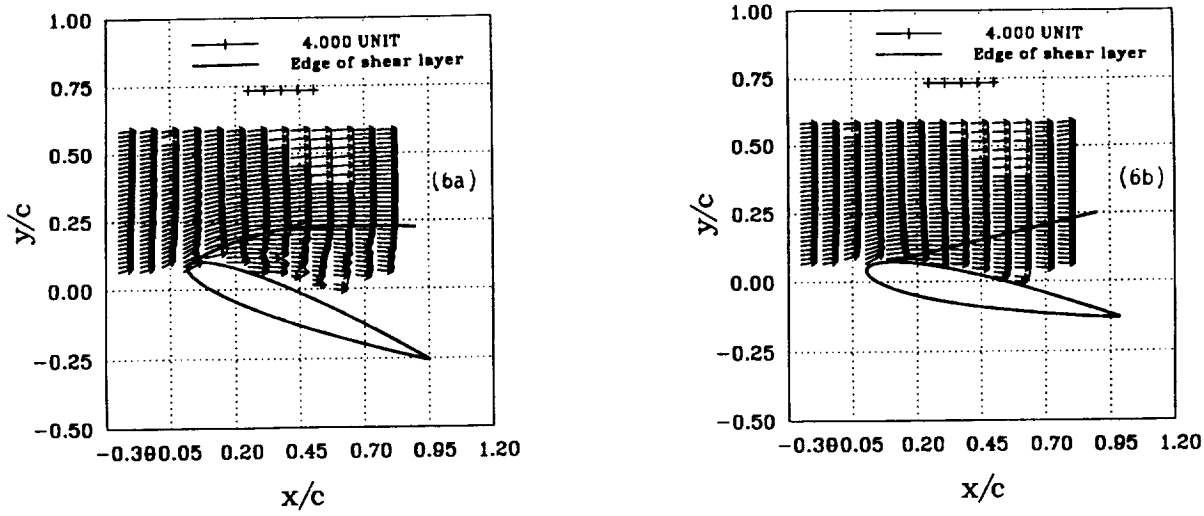

Fig. 6. Absolute Velocity Distribution: (a) $\alpha = 20.0°$, (b) $\alpha = 10.0°$.

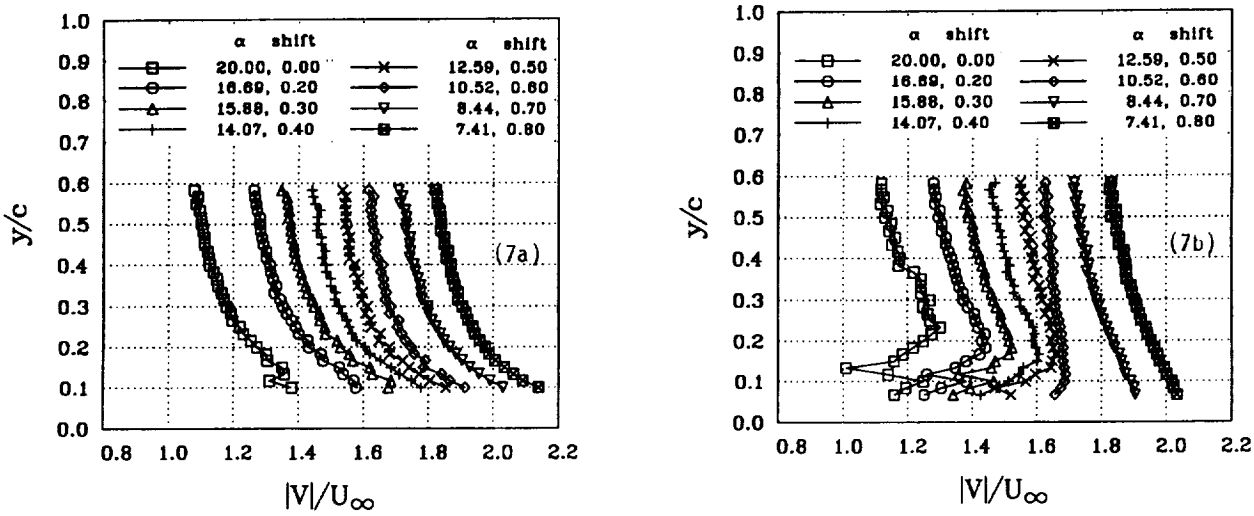

Fig. 7. Absolute Velocity Distributions with α : (a) x/c = 0.083, (b) x/c = 0.250.

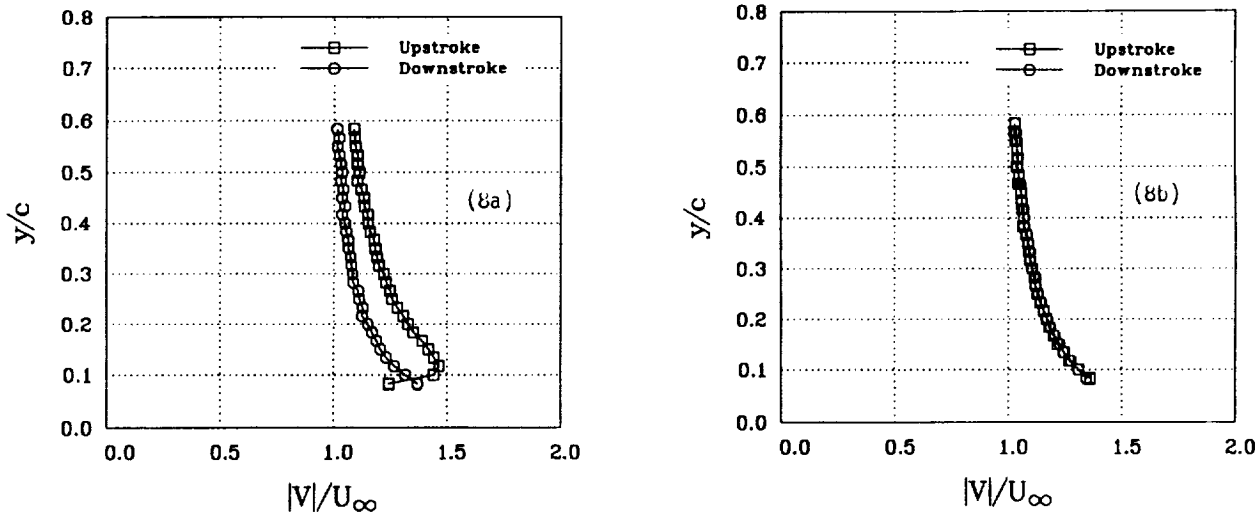

Fig. 8. Comparison of Absolute Velocity Distribution: (a) $\alpha = 10.0°$, (b) $\alpha = 5.46°$.

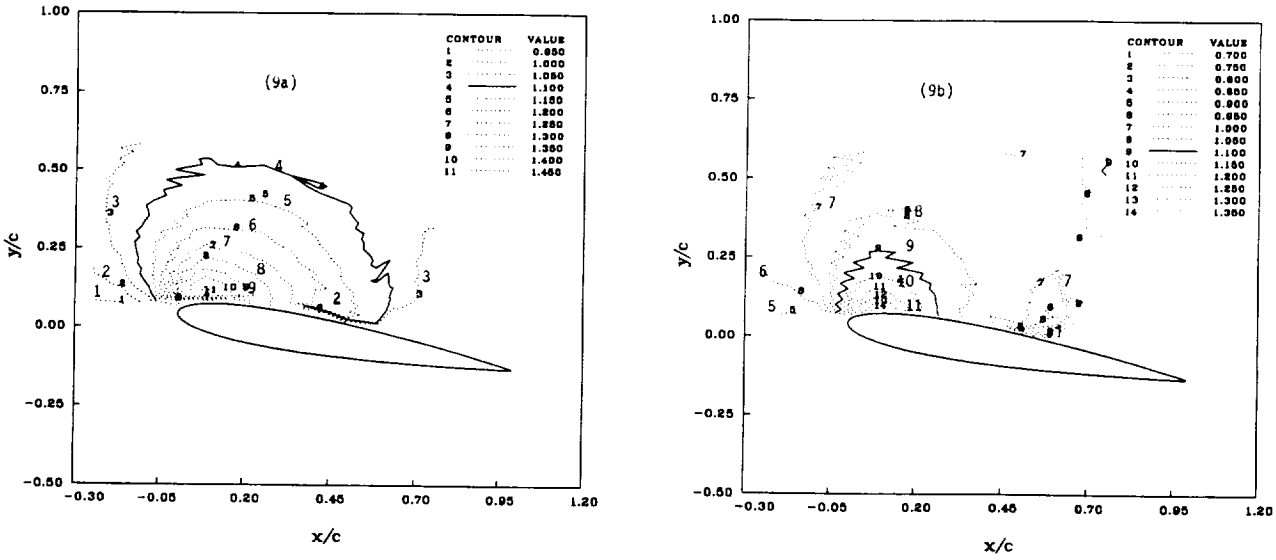

Fig. 9. Contours of Absolute Velocity at $\alpha = 10.0°$: (a) Upstroke, (b) Downstroke.

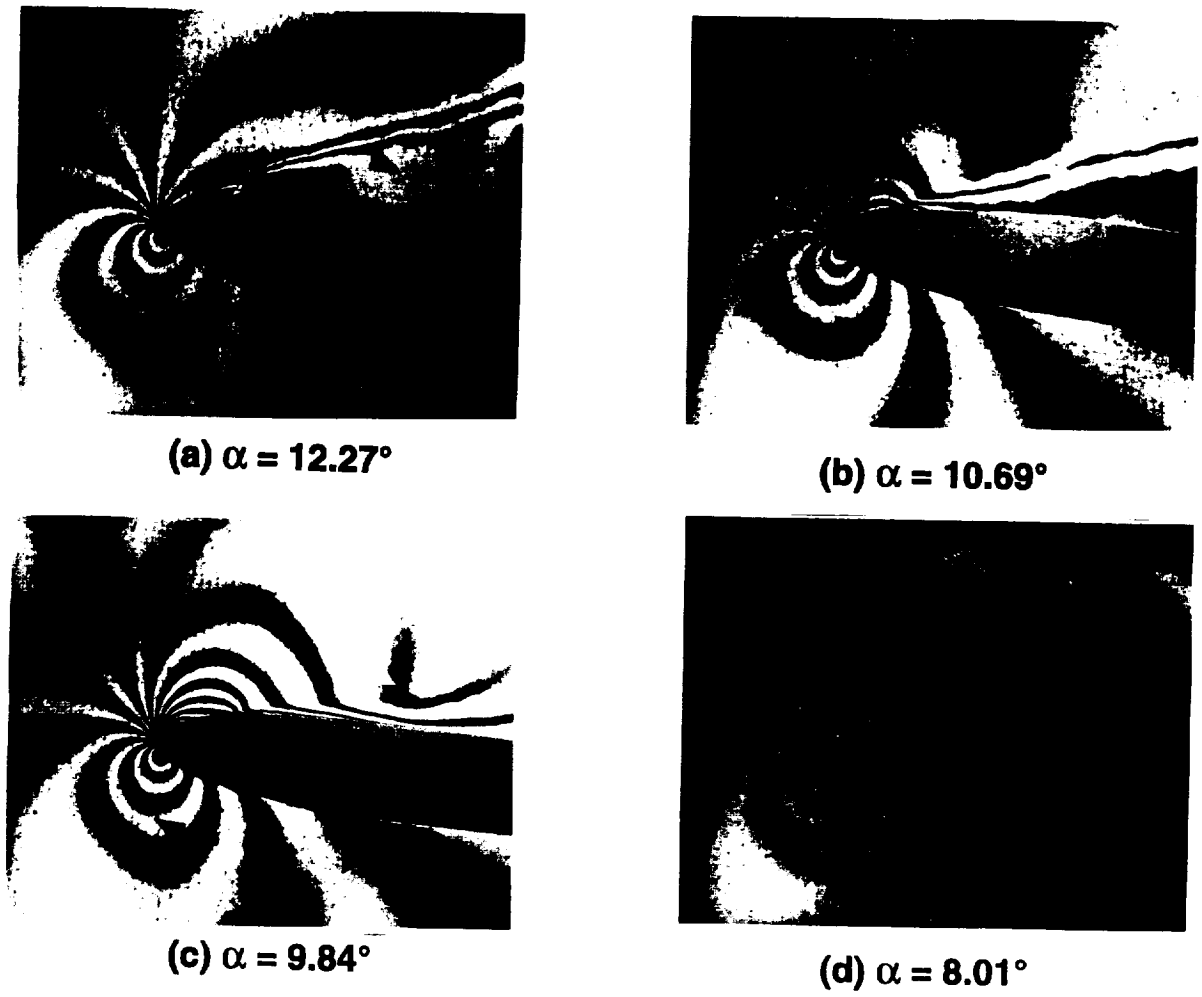

Fig. 10. Interferograms of Reattachment Process.

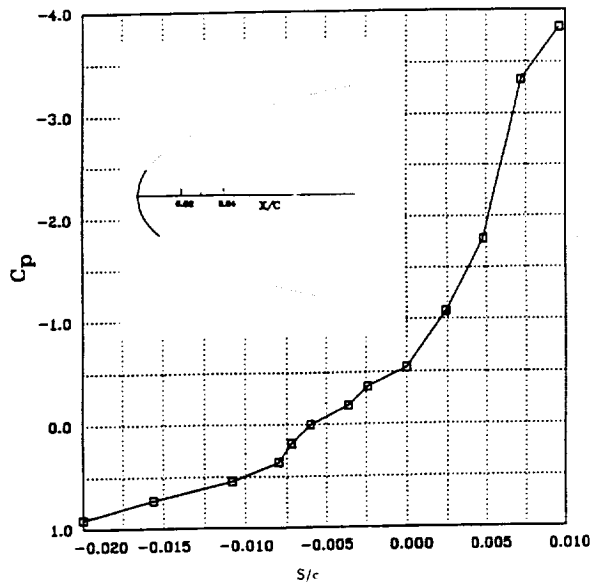

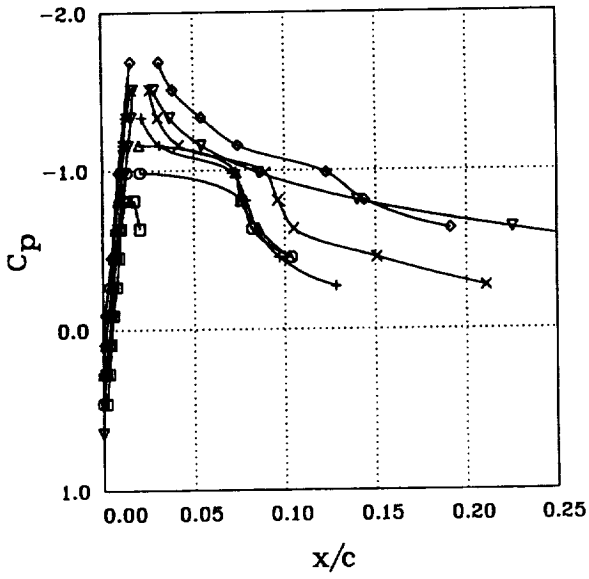

Fig. 12. Pressure Distribution During Reattachment Process.

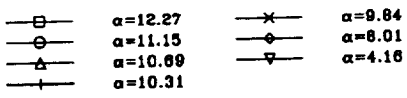

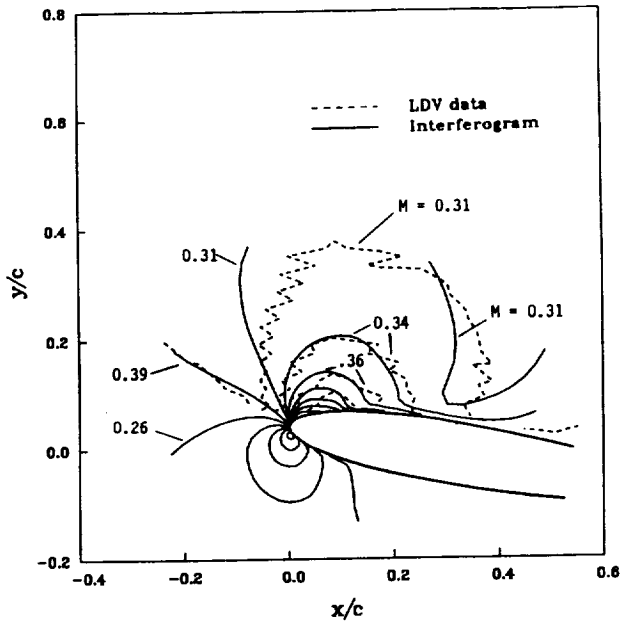

Fig. 13. Comparison of LDV Data with the Interferogram at $\alpha = 10.0°$.

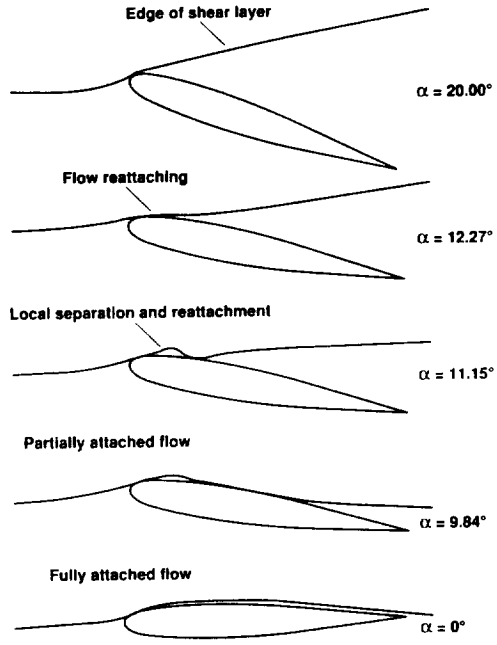

Fig. 14. Schematic of the Reattachment Process.

APPENDIX D